NUMERICAL SIMULATION OF TURBULENT FLOW OVER L-SHAPED RIBLETS WITH A MODIFIED TWO-EQUATION TURBULENCE MODEL

Hyon Kook Myong
School of Mechanical and Automotive Engineering
Kookmin University
Chongnung-dong 861-1, Songbuk-ku, Seoul 136-702, Korea

ABSTRACT

The paper reports the outcome of a numerical simulation of turbulent flow over L-shaped riblets obtained by using a modified two-equation turbulence model. In the present paper, a modified version of the low-Reynolds-number $k-\varepsilon$ model of Launder & Sharma (1974, LS hereafter) is introduced, in which the gradient production term of ε-equation is modeled to have only the normal derivative terms, and applied to the flows over the L-shaped riblets with finite thickness. And then systematical analysis is made on turbulence quantities. Compared to the original LS model, the present model has the drag reduction behavior and the flow field structure in better accord with both experimental results and the recent DNS results by Choi et al. (1993).

INTRODUCTION

The wall surfaces mounted with longitudinal micro-grooves, commonly termed 'riblets', are recognized as a efficient device for the drag reduction purpose. Recently, Choi et al. (1993, CMK hereafter) have applied successfully DNS (Direct Numerical Simulation) to the turbulent flow over riblet-mounted surfaces. Their results are consistent, at least qualitatively, with the available experimental data (e.g. Walsh, 1982). However, DNS is applicable to only low-Reynolds-number flows. Hence, a parametric study by DNS, which is requires large computer memory and computational time, is hardly possible for practical flows. Numerical computation with turbulence models may be considered as an alternative, since its cost is moderate compared with that of experiments or DNS.

To predict the riblet flows, Launder & Li (1993) have adopted the LS model, in which proximity to the wall is sensed only via the local value of a turbulent Reynolds number. The qualitative performance of riblets in reducing drag is fairly well captured. However, their numerical results for L-shaped riblets have shown that the maximum drag reduction is 22.5 %, which is 50% greater than hitherto claimed for V-grooves, and also its location occurs at the level of $h^+ (\equiv u_\tau h/\nu)$ at least three times larger than is usually found in experiments (see Fig. 1 and Fig. 2).

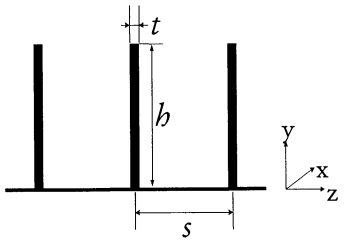

Fig. 1 Cross –sectional view of riblet configurations.

Recently, Myong (1997, 1998a, b) has pointed out that the original LS model does not work properly when there are strong gradients in two or three directions of turbulence quantities as in case of the flows over riblets. And he has modified the LS model without affecting its level under two-dimensional straining in which it has been calibrated, and applied the modified model to the flows over idealized L-shaped riblets with zero thickness. Compared to the original LS model, the modified model is found to improve the accuracy of the prediction for drag reduction behavior. However, the shape of these zero thickness riblets differs from the actual 'thin-element' riblets of which the rib thickness is at least 8% of the rib height.

In the present paper, the author's modified LS model is briefly introduced and applied to the turbulent flows over the L-shaped riblets with finite thickness. And then systematical analysis is made on turbulence quantities. Note here that secondary motions reported by DNS are not generated by the present method, since the latter method uses an isotropic $k-\varepsilon$ model adopting an eddy viscosity concept. The present study thus aims for investigating whether the isotropic $k-\varepsilon$ model can successfully predict drag reductions in line with experimental observations.

MATHEMATICAL MODELS

The present study is focused on the fully developed turbulent flow between parallel planes extended infinitely, one of which is mounted with L-shaped riblets as shown Fig. 1. The L-shaped riblet is numerically the simplest case since it may be studied using a Cartesian-grid system. The choice of an infinite plane channel also allows to reduce considerable computational cost, since the computations are then two-dimensional that can be solved on a single plane orthogonal to the mean flow. A further advantage of a channel flow study is that the results are cleaner: there is no streamwise variation of wall friction or shear layer thickness as there is in boundary layer flow. The different contributions of the influential parameters can thus be separately assessed.

In the present study, the author's modified LS model is used to calculate turbulence quantities. Compared with the original LS model, the last underlined term, (i.e. the gradient production term) on the right hand side of the following $\varepsilon-$ equation is only modified with the same as model coefficients and functions as the standard values and forms of the original LS model:

$$0=\frac{\partial}{\partial x_j}\left[\left(\nu+\frac{\nu_t}{\sigma_\varepsilon}\right)\frac{\partial\tilde{\varepsilon}}{\partial x_j}\right]+C_{\varepsilon 1}\frac{\tilde{\varepsilon}}{k}P_k-C_{\varepsilon 2}f_{\varepsilon 2}\frac{\tilde{\varepsilon}^2}{k}$$
$$\underline{+2\nu\nu_t\delta_{jk}\left(\frac{\partial^2 U_i}{\partial x_j\partial x_k}\right)^2} \qquad (1)$$

Note that the original form of the fourth term, $2\nu\nu_t\left(\partial^2U_i/\partial x_j\partial x_k\right)^2$ includes the cross derivative term which is removed in the present model. Myong (1997, 1998a, b) has recently recognized that this cross derivative term can have physically unreasonably large values in the region where there are strong y-gradients as well as z-gradients in U. In fact, in the region immediately above the riblets, there are strong gradients both in mean velocity and in k and $\tilde{\varepsilon}$ in both the y- and z directions. These strong lateral inhomogeneities enhance the dissipation rate within the semi-viscous near-wall region through this cross derivative term. An enhancement of dissipation rates would effectively extend the viscosity-affected sublayer to somewhat greater values of $y^+(\equiv u_\tau y/\nu)$, thus reducing drag too much. Consequently, the original LS model overestimates the drag reduction. Note also here that the present model given by Eq. (1) does not affect its level under 2-dimensional straining in which the term has been calibrated, since in a simple shear flow the last term of the equation is reduced to $2\nu\nu_t\left(\partial^2U/\partial y^2\right)^2$.

Note here that, although the original model form of the gradient production term is widely used and more rational than the last term of Eq. (1), it has not ever been applied to the flows where the cross derivative term is dominant compared with the other normal derivative terms. Thus, the proper modeled form for the gradient production term is still open to debate.

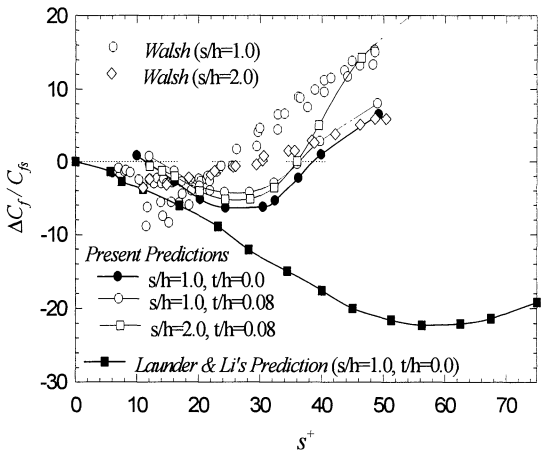

Fig.2 Skin friction coefficient variations over riblets.

NUMERICAL METHODS

In the present study, the actual L-shaped riblets with thin-element (t/h=0.08) are tested.

Since the riblet surfaces are usually embedded in the near-wall layer, the half-width H of the channel is fixed to be 25 and 50 times the riblet height h in the present study. The computations are performed for two different geometric ratios, i.e., s/h=1 and 2, and for a bulk Reynolds number Re varying from 12000 to 90000, which is based on the mean velocity and the channel width. Typical mesh densities of 240 x 48 for s/h=1 and 240 x 68 for s/h=2, respectively, are used to cover the computational region. It covers between the two parallel plates (y-direction) and, from left to right the vertex of one riblet and the midway floor between riblets (z-direction). A particularly dense grid is also given near the riblet tip to resolve the velocity gradient with accuracy.

As the boundary conditions, zero-gradient conditions are applied for all the dependent variables at the symmetry planes, and all the dependent variables are conveniently set to zero at the walls.

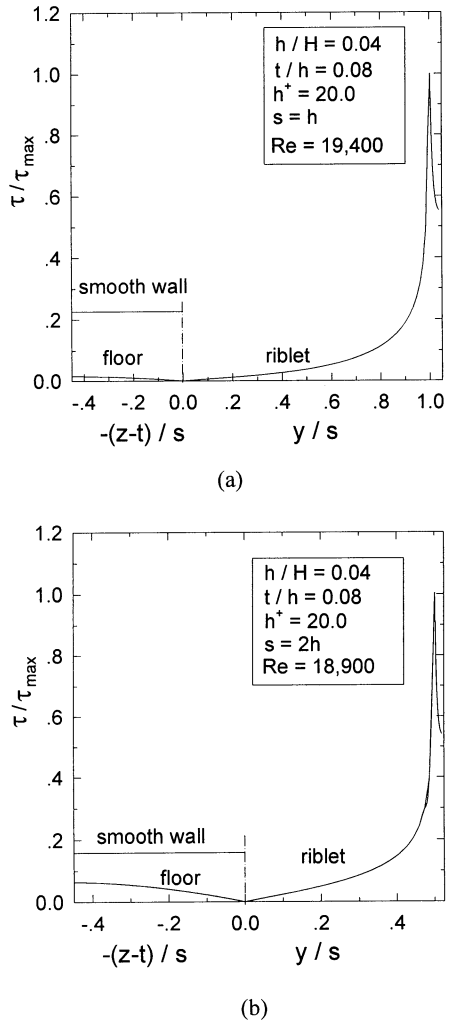

Fig. 3 Local skin friction distributions along the rigid surface. (a) drag reduction case; (b) drag increase case.

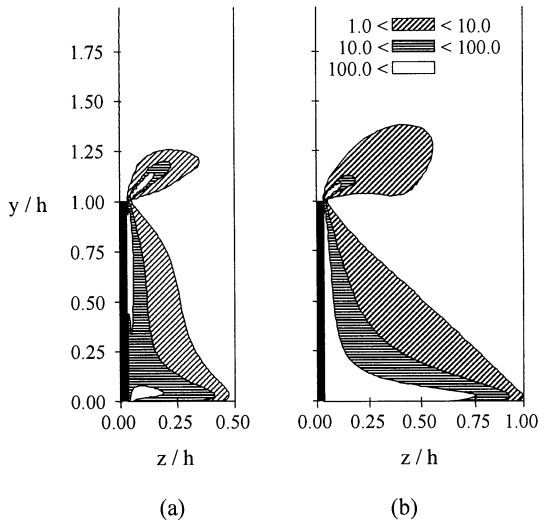

Fig. 4 Relatively dominant region of cross-derivative term in the gradient production term in ε-equation. . (a) drag reduction case (h/H=0.04, t/h=0.08, s=h, s^+=20, Re=19,400): (b) drag increase case (h/H=0.04, t/h=0.08, s=2h, s^+=40, Re=18,900).

COMPUTED BEHAVIOR AND DISCUSSIONS

Riblet Performances

The relative change of the skin friction coefficient is shown in Fig. 2 as a function of $s^+ (\equiv u_\tau s/\nu)$. For comparison, the result predicted by Launder & Li (1993) for an idealized riblet with zero thickness is also included, where the Reynolds number is fixed to 50000 while the height of riblet h is allowed to vary. The Launder & Li's numerical prediction clearly shows that the original LS model overestimates the drag reduction. On the other hand, for the same case, i.e. s/h=1 and t/h=0 with $H/h = 25$ the present model predicts a maximum drag reduction of 6 ~ 7 % and the optimum reaching at $s^+ \approx 25$ ($h^+ \approx 25$). The present model is thus able to predict the trend and the magnitude of the experimental results excellently well, although it predicts drag reduction a little large over the range of s^+ greater than 20.

For the realistic practical riblet with $t/h = 0.08$ the present model predicts maximum drag reductions of 4.5% for s/h=1, 5.5% for s/h=2 with $H/h = 25$, and 6.4% for both cases with $H/h = 50$, indicating the slight dependence of the maximum drag reductions on both Reynolds number and riblet geometry. These results are in good accord with the experiments, while the optimum is still reached at $s^+ \approx 25$ for both s/h=1 and s/h=2. The present results also confirm partly the Launder & Li's conjecture that the additional surface area (the finite thickness) on top of the riblet exposed to high velocity fluid would have the effect of somewhat reducing the attainable drag reduction.

Flow Field Structure

The change of flow field structure is examined below by comparing two different flow conditions. For both cases of the flow conditions the values of h^+=20, h/H=0.04 and $t/h = 0.08$ are fixed, and the geometric ratios of s/h are only changed to 1 and 2. The two conditions correspond to the drag reducing and increasing conditions, respectively, as shown in Fig. 2. In the present work, about 3.5 % reduction and 5 % increase in the skin friction are obtained for $s^+ \approx 20$ and $s^+ \approx 40$, respectively, while 4 % reduction and 3 % increase in Walsh (1982) and 6 % reduction and 2 % increase in CMK, respectively, are obtained for the V-groove riblet surface.

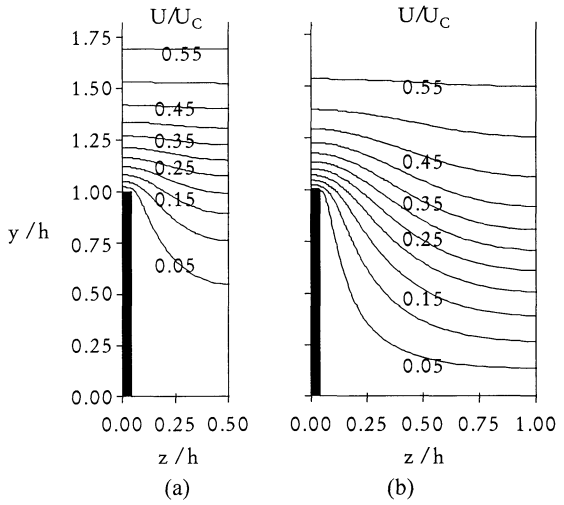

Fig.5 Contours of predicted streamwise velocities around the riblet. (a) drag reduction case (h/H=0.04, t/h=0.08, s=h, s^+=20, Re=19,400); (b) drag increase case (h/H=0.04, t/h=0.08, s=2h, s^+=40, Re=18,900).

Figure 3 shows the predicted local skin friction distributions around the tip of the riblet for both the cases of $s/h=1.0$ and $s/h=2.0$ with t/h=0.08. For both cases, the results show that a low level of shear stress decreases gradually as one proceeds from the mid-plane between two adjacent riblets to the center. On the other hand, the shear stress increases rapidly when the tip of the riblet is approached and then somewhat decreases with leading to a higher level of shear stress being distributed along the riblet surface and especially concentrated near the tip of the riblet. The predicted profiles of local skin friction clearly show that, although the thickness is only 8% of the riblet height, the high concentration of the skin friction around the tip of the riblet make this small amount of additional wetted area count in integrating the local wall shear stresses. With this type of distribution one may thus conclude that by introducing the riblet the wetted area of the channel is increased, but it is the riblet surface near the tip that carries the great majority of the friction drag.

One more important fact may be guessed on the drag reduction mechanism from Fig. 3. In the case of Fig. 3(a), the wall shear stresses in the floor from the mid-plane between the two adjacent riblets to the corner have far smaller portions of the total drag than those in the case of Fig. 3(b). Note that the results of figure 3(a) and 3(b) are the drag reducing and increasing cases in figure 2, respectively. One of possible explanations for the drag reduction mechanism is as follows; the skin friction reduction associated with the riblet valleys (midway between riblets) exceeds the skin friction increase associated with the riblet tips, thus yielding an overall skin friction reduction.

Figure 4 shows the region where the cross derivative term

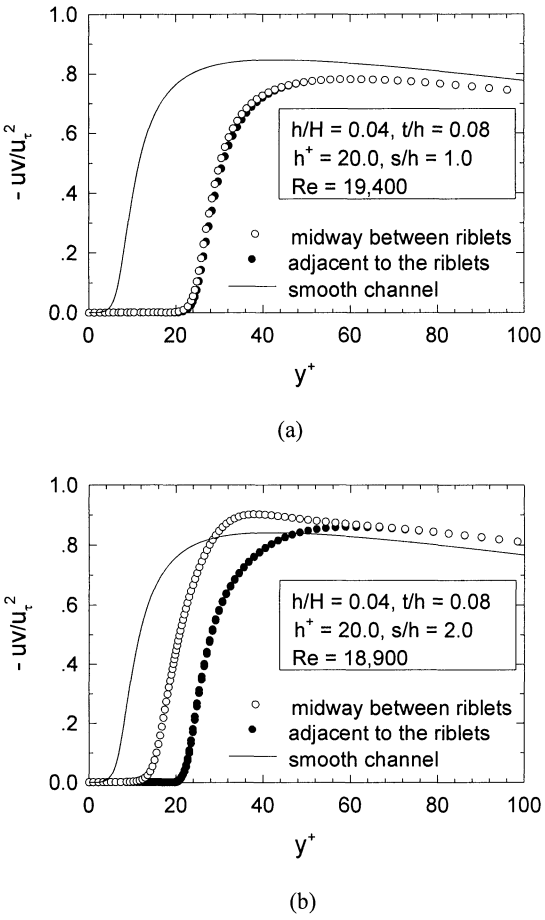

Fig.6 Predicted Reynolds stress profiles in wall coordinates. (a) drag reduction case; (b) drag increase case.

is relatively dominant with respect to the other normal derivative terms in the last term of Eq. (1), i.e. the gradient production term. Note that these results are obtained from the prediction of the present model having only the normal derivative terms. The cross derivative term is found to have physically unreasonably large values in both the regions above the top of the riblet and in the cavity region. As discussed previously these strong lateral inhomogeneities enhance the dissipation rate within the semi-viscous near-wall region through this cross derivative term and then an enhancement of this dissipation rates would effectively extend the viscosity-affected sublayer to somewhat greater values of y^+, thus reducing drag too much. This result therefore clearly demonstrates that the original LS model overestimates the drag reduction compared with the present model, as can be seen in Fig. 2.

The detailed velocity profiles around the riblet obtained for the two cases are presented in Fig. 5. For both cases, the wall shear stresses are concentrated around the riblet tips

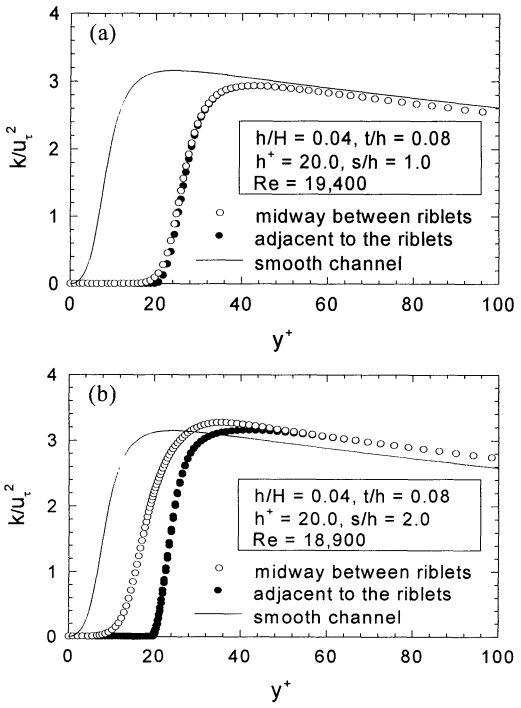

Fig.7 Predicted turbulent kinetic energy profiles. (a) drag reduction case; (b) drag increase case.

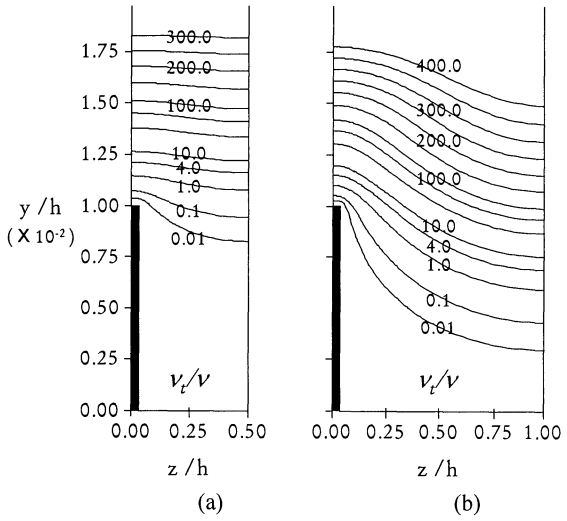

Fig. 8 Predicted contours of turbulent viscosity around the riblet. (a) drag reduction case (h/H=0.04, t/h=0.08, s=h, s^+=20, Re=19,400): (b) drag increase case (h/H=0.04, t/h=0.08, s=2h, s^+=40, Re=18,900).

and the spanwise variations due to the existence of the riblet limit only near the riblet. There exist, however, large differences in these two plots. In the case $s^+ \approx 40$, the constant velocity lines are penetrating deeper and more intensified near the tip of the riblet, which might suggest that the total viscous drag for $s^+ \approx 40$ is larger than that for $s^+ \approx 20$.

The Reynolds shear stress profiles are shown in Fig. 6. In the case $s^+ \approx 20$, the maximum Reynolds shear stress above the riblets is reduced by 10 % as compared with that above the flat plate, and there is negligible spanwise variation of the Reynolds shear stress near the riblets. Walsh (1980) and CMK reported the maximum reductions of 16 % and 12 % in the Reynolds shear stress above riblets for the V-groove riblet surface, respectively. In the case $s^+ \approx 40$, however, the maximum Reynolds shear stress above the riblets is significantly increased above the mid-plane between riblets and is nearly unaffected above the riblet tip as compared with the flat-plate side. In this case, there is also substantial spanwise variation of $-uv$ near the riblets; peak locations and magnitudes of the Reynolds shear stress above the riblet tip and the midway floor between riblets differ greatly from the flat plate profile. These observations have also been clearly reported in CMK's DNS studies, although the maximum Reynolds shear stress is significantly increased above the riblet tip contrary to the present results.

Predicted profiles of turbulent kinetic energy k in wall coordinates are shown in Fig. 7. Maximum turbulent kinetic energy is reduced by 10 % in the case $s^+ \approx 20$, but in the case $s^+ \approx 40$, it is increased above the midway between riblets and is nearly unaffected above the riblet tip as compared with the flat-plate side. CMK also reported from the DNS study the maximum reductions of 10% in the turbulent kinetic energy above riblets for the V-groove riblet. In the case $s^+ \approx 40$, there is also substantial spanwise variation of k near the riblets; peak locations and magnitudes of the turbulent kinetic energy above the riblet tip and the midway floor between riblets differ greatly from the flat plate profile. These observations have also been clearly reported in CMK's DNS studies.

Finally, Fig. 8 shows contours of the turbulent viscosity around the riblet. One may notice that the flow within the riblet cavity is essentially laminarized, even for the case $s^+ \approx 40$. On the plane just above the riblet tip the maximum turbulent viscosity ν_t on the line midway between adjacent riblets is only about 2.0 times the laminar viscosity. In the case $s^+ \approx 20$ the flow is even more laminarized with all the values of ν_t being less than 5 % inside the riblet cavity. The laminarization is due to the reduced level of turbulent kinetic energy as shown in Fig. 7 within the riblet cavity for those two riblets. Consequently, this directly explains why the great majority of the drag arises from the region near the tip of the riblet as already shown in figures 3(a) and 3(b), although the surface area of the riblet is greatly enhanced relative to that of a smooth surface. Also, from the model's prediction a possible drag mechanism is that riblets produce a modest thickening of the

viscous sublayer and that this leads to a reduction in friction sufficient to compensate for the increased wetted area.

CONCLUSIONS

In the present study, the author's modified LS model is briefly introduced, in which the gradient production term of ε-equation is modeled to have only the normal derivative terms, without affecting the original LS model's level under 2-dimensional straining in which it has been calibrated. Then, the actual L-shaped (blade-type) riblets with finite thickness have been examined. Compared to the original LS model, the present model has predicted the greatly improved drag reduction behavior for this geometry, which is in good accord with experiment though the optimum value of the riblet height for the maximum drag reduction is predicted to be slightly larger than measurements indicate.

Turbulence statistics above the riblets are computed and compared with those above a flat plate. Differences in the mean velocity profile and turbulence quantities are found to be limited to the inner region of the boundary layer. The Reynolds shear stress and the turbulent kinetic energy as well as the mean velocity above the riblet are reduced in drag-reducing configurations. The present predictions are in good agreement with the recent DNS results by Choi et al. (1993).

ACKNOWLEDGEMENTS

This work has been supported by the Korea Science and Engineering Foundation (KOSEF) through the Advanced Fluids Engineering Research Center (AFERC) at the Pohang University of Science and Technology (POSTECH).

REFERENCES

Choi, H., Moin, P. & Kim, J., 1993, "Direct Numerical Simulation of Turbulent Flow over Riblets." *J. Fluid Mech.*, Vol.255, pp.503-539.

Launder, B. E. & Li, S. P., 1993, "On the Prediction of Riblet Performance with Engineering Turbulence Models." *Appl. Sci. Res.*, Vol.50, pp.283-298.

Launder, B. E. & Sharma, B. I., 1974, "Application of the Energy Dissipation Model of Turbulence to the Calculation near a Spinning Disc." *Letters in Heat and Mass Trans*fer, Vol.1, pp.131-138.

Myong, H. K., 1997, "Computation of a Turbulent Flow over a Riblet Surface for Drag Reduction." *Report of Transport Vehicle Flow Research Division*, AFR-96-A03, pp.39-66, AFERC, POSTECH, Korea.

Myong, H. K., 1998a, "Prediction of Turbulent Flow over L-shaped Riblet Surfaces with $k-\varepsilon$ Turbulence Models." (in Korean) *Trans. Korean Soc. of Mech. Eng.*, Vol.22, No.1, pp.93-103.

Myong, H. K., 1998b, "Computation of Turbulent Flow over L-shaped Riblets with Two-Equation Turbulence Models." *Proc. Of 4th KSME-JSME Fluids Eng. Conf.*, Haeundae, Pusan, Korea, October 18-21, pp.657-660.

Walsh, M. J., 1980, "Drag Characteristics of V-groove and Transverse Curvature Riblets." In Viscous Drag Reduction (ed. G. R. Hough), AIAA.

Walsh, M. J., 1982, "Turbulent Boundary Layer Drag Reduction using Riblets." *AIAA Paper No.* 82-0169.